Supporting Information

Synthesis–Structure Relationships in Li- and Mn-rich Layered Oxides: Phase Evolution, Superstructure Ordering and Stacking Faults

Ashok S. Menon, Said Khalil, Dickson O. Ojwang, Kristina Edström, Cesar Pay Gomez and William R. Brant*

Department of Chemistry-Ångström Laboratory, Uppsala University, Box 538, SE-75121 Uppsala, Sweden

Corresponding Author: William R. Brant (william.brant@kemi.uu.se)

Contents

1. Structure models used to simulate XRD patterns in Fig. 1c of the manuscript

Table S1: Structure model for Li_2MnO_3 (B_{iso} is the isotropic thermal displacement parameter)

a (Å)	**b (Å)**	**c (Å)**	**β (°)**			
4.9292	8.5315	5.02510	109.337			
Space group: *C*2/*m*						
			Atomic positions and occupancies			
Atom	**Wyckoff position**	**x/a**	**y/b**	**z/c**	**Occupancy**	**B_{iso}**
Mn	4*g*	0	0.1687	0	1	0.5
Li	2*b*	0	0.5	0	1	0.5
Li	4*h*	0	0.681	0	1	1.0
Li	2*c*	0	0	0.5	1	1.0
O	4*i*	0.224	0	0.225	1	0.8
O	8*j*	0.253	0.323	0.2275	1	0.8

Table S2: Structure model for $Li_{1.2}Mn_{0.6}Ni_{0.2}O_2$

a (Å)	**b (Å)**	**c (Å)**	**β (°)**			
4.9292	8.5315	5.02510	109.337			
Space group: *C*2/*m*						
			Atomic positions and occupancies			
Atom	**Wyckoff position**	**x/a**	**y/b**	**z/c**	**Occupancy**	**B_{iso}**
Mn	4*g*	0	0.1687	0	0.9	0.5
Ni	4*g*	0	0.1687	0	0.1	0.5
Li	2*b*	0	0.5	0	0.6	0.5
Ni	2*b*	0	0.5	0	0.4	0.5
Li	4*h*	0	0.681	0	1	1.0
Li	2*c*	0	0	0.5	1	1.0
O	4*i*	0.224	0	0.225	1	0.8
O	8*j*	0.253	0.323	0.2275	1	0.8

Table S3: Structure model for $Li_{1.2}Mn_{0.54}Ni_{0.13}Co_{0.13}O_2$ (adapted from Whitfield *et al.*)[1]

a (Å)	**b (Å)**	**c (Å)**	**β (°)**			
4.9292	8.5315	5.02510	109.337			
Space group: *C*2/*m*						
			Atomic positions and occupancies			
Atom	**Wyckoff position**	**x/a**	**y/b**	**z/c**	**Occupancy**	**B_{iso}**
Mn	4*g*	0	0.1687	0	0.7000	0.5
Ni	4*g*	0	0.1687	0	0.1150	0.5
Co	4*g*	0	0.1687	0	0.1700	0.5
Li	4*g*	0	0.1687	0	0.015	0.5
Li	2*b*	0	0.5	0	0.6	0.5
Ni	2*b*	0	0.5	0	0.16	0.5
Co	2*b*	0	0.5	0	0.19	0.5
Mn	2*b*	0	0.5	0	0.05	0.5
Li	4*h*	0	0.681	0	1	1.0
Li	2*c*	0	0	0.5	1	1.0
O	4*i*	0.224	0	0.225	1	0.8
O	8*j*	0.253	0.323	0.2275	1	0.8

2. Single peak fitting results

The peak at ~44.5° in the XRD data was fit using Topas[2]. The emission profile and instrumental broadening (using the modified Thompson-Cox-Hastings pseudo-Voigt peak shape function) was obtained by fitting the LaB_6 data, as in Pawley refinement. A second-degree Chebyshev polynomial was used to model the background. Sample-dependent broadening was modelled through a pseudo-Voigt function, whose Gaussian and Lorentzian contributions were calculated using the "CS_G" and "CS_L" macros in Topas. The refined values were used to calculate the coherently diffracting domain size (nm) as defined in Balzar *et al* (as volume average column height).[3]

Table S4: Results of the single peak fitting.

Sample	R_{wp}	Peak position	Intensity	Domain size (nm)
SG-LMO	3.50946	44.73364(37)	297(1)	43.82(44)
SG-LMNO	3.27390	44.49316(50)	489(2)	27.20(17)
SG-LMNCO	5.74405	44.69276(83)	393(3)	31.91(47)
SS-LMO	7.16304	44.75160(87)	280(2)	37.95(45)
CP-LMNO	5.32026	44.47905(66)	455(3)	42.29(82)
CP-LMNCO	2.82814	44.61100(35)	503(2)	44.08(67)

3. XRD data – $001_{C2/m}$ reflection of the samples

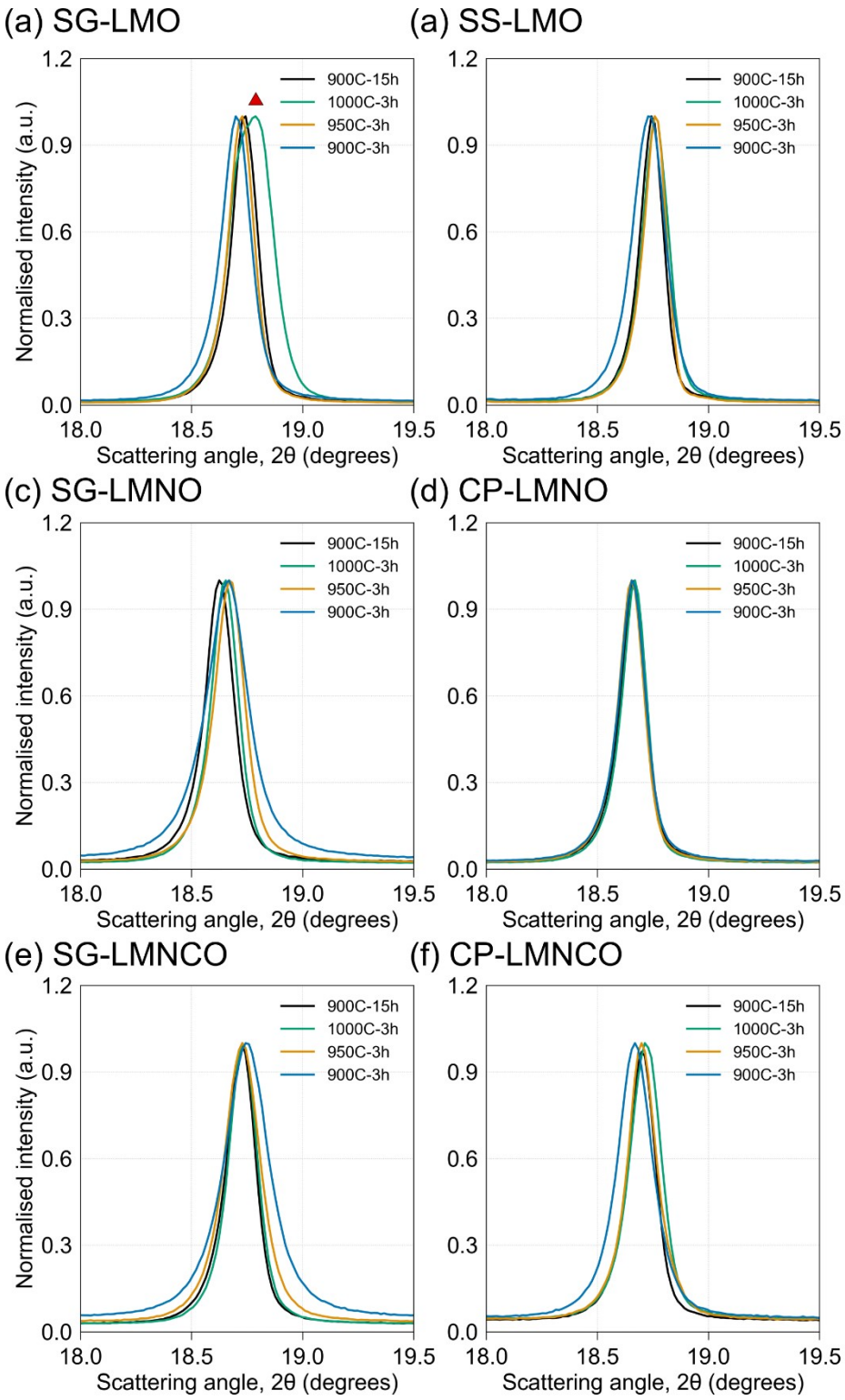

Figure S1: Magnified view of the 001 reflection from the XRD dataset. In (a), the formation of the spinel phase is highlighted using a red triangle.

4. Compositional analyses using ICP–OES

Tables S5–S7 contain the cation concentration of all the samples expressed as mole fractions. The mole fraction of each constituent element as expected from the formula is highlighted.

Table S5: Elemental composition of sol-gel (SG) and solid-state (SS) Li_2MnO_3 (LMO) samples.

Sample		Li	Mn
LMO (expected)		0.667	0.333
SG-LMO	900C-3h	0.66(1)	0.339(8)
	950C-3h	0.66(1)	0.340(7)
	1000C-3h	0.65(2)	0.348(7)
	900C-15h	0.66(1)	0.339(8)
SS-LMO	900C-3h	0.67(2)	0.32(2)
	950C-3h	0.67(4)	0.33(1)
	1000C-3h	0.66(1)	0.333(9)
	900C-15h	0.66(2)	0.333(9)

Table S6: Elemental composition of sol-gel (SG) and coprecipitated (CP) $Li_{1.2}Mn_{0.6}Ni_{0.2}O_2$ (LMNO) samples.

Sample		Li	Mn	Ni
LMNO (expected)		0.6	0.3	0.1
SG-LMNO	900C-3h	0.58(1)	0.314(9)	0.104(1)
	950C-3h	0.58(1)	0.311(7)	0.106(3)
	1000C-3h	0.58(2)	0.31(1)	0.108(3)
	900C-15h	0.60(2)	0.30(1)	0.099(3)
CP-LMNO	900C-3h	0.61(1)	0.29(1)	0.102(2)
	950C-3h	0.60(1)	0.297(7)	0.101(3)
	1000C-3h	0.60(2)	0.30(1)	0.098(2)
	900C-15h	0.60(2)	0.30(1)	0.100(3)

Table S7: Elemental composition of sol-gel (SG) and coprecipitated (CP) $Li_{1.2}Mn_{0.54}Ni_{0.13}Co_{0.13}O_2$ (LMNCO) samples.

Sample		Li	Mn	Ni	Co
LMNCO (ideal)		0.6	0.27	0.065	0.065
SG-LMNCO	900C-3h	0.59(2)	0.274(5)	0.068(1)	0.073(2)
	950C-3h	0.60(2)	0.260(5)	0.064(1)	0.071(1)
	1000C-3h	0.581(5)	0.274(6)	0.069(1)	0.074(1)
	900C-15h	0.59(2)	0.266(8)	0.066(2)	0.073(2)
CP-LMNCO	900C-3h	0.60(2)	0.27(2)	0.066(2)	0.068(3)
	950C-3h	0.60(3)	0.27(1)	0.066(2)	0.067(2)
	1000C-3h	0.59(2)	0.274(7)	0.069(1)	0.069(2)
	900C-15h	0.59(2)	0.27(1)	0.067(2)	0.069(3)

5. Pawley refinement results

Pawley refinement[4] of a monoclinic *C*2/*m* unit cell was performed against XRD data using TOPAS software. The emission profile and instrumental peak broadening was calculated using data collected from a NIST SRM 660c LaB_6 standard reference material. A modified Thompson-Cox-Hastings pseudo-Voigt peak shape function ("TCHZ_Peak_Type") together with a function for the peak asymmetry ("Simple_Axial_Model") was used to model the instrumental broadening. For the unit cell refinements, an additional "TCHZ_Peak_Type" peak shape function was used to model the sample broadening. The "Simple_Axial_Model" was also allowed to refine due to the presence of the Bragg reflections at angles lower than that contained in the data from the standard sample. A 6th degree Chebyshev polynomial was used to fit the background.

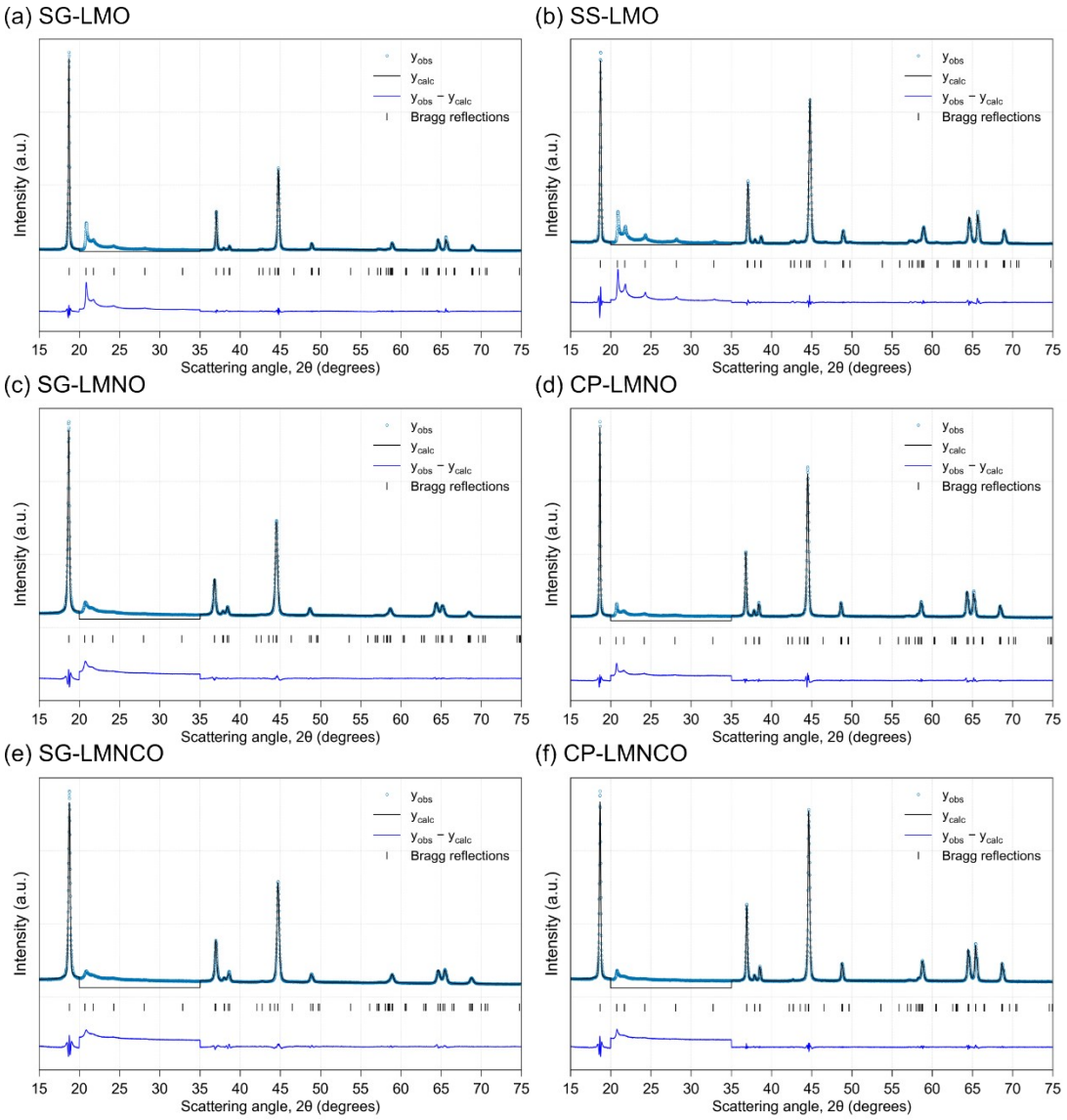

Figure S2: Pawley refinement plots of the different samples synthesised by annealing at 900 °C for 3 h (900C-3h).

Table S8 shows the refined *C*2/*m* unit cell parameters of the 900C-3h samples. A common trend is observed for the *a* and *b* lattice parameters and the unit cell volume: LMNO>LMNCO>LMO. The higher *a* and *b* parameters in LMNO are due to the larger amount of Ni^{2+} which has a higher ionic radius of ~0.69 Å. Expectedly, the replacement of Ni^{2+} with the smaller Co^{3+} (~0.545 Å) leads to the lower values seen in LMNCO. The *c* lattice parameter is representative of the inter-layer distance and the lower *c* value for LMNCO indicates that the Co^{3+} facilitates in a more compact packing of the Li- and TM-layers. Therefore, the addition of Ni^{2+} into the LMO structure leads to its significant expansion, which is then partly mitigated by the introduction of Co^{3+} in LMNCO.

Table S8: Refined lattice parameters of a monoclinic (*C*2/*m*) unit cell obtained through Pawley refinement against XRD data for the samples synthesised by annealing at 900 °C for 3 h (900C-3h). R_{wp} and GoF denote the R-weighted pattern and goodness of fit, respectively, and are defined in the TOPAS Academic technical reference manual.

Sample	**R_{wp}**	**GoF**	**a (Å)**	**b (Å)**	**c (Å)**	**β (°)**	**Vol. (Å^3)**
SG-LMO	7.1	2.7	4.9227(4)	8.5302(4)	5.0149(1)	109.248(3)	198.82(2)
SS-LMO	8.2	2.6	4.9231(3)	8.5251(5)	5.0206(2)	109.290(3)	198.89(2)
SG-LMNO	5.3	2.8	4.9460(9)	8.591(1)	5.0257(3)	109.36(1)	201.46(5)
CP-LMNO	4.8	2.4	4.9525(5)	8.5852(4)	5.0326(1)	109.321(3)	201.93(2)
SG-LMNCO	5.5	2.9	4.9284(3)	8.573(2)	5.0050(4)	109.36(1)	199.52(4)
CP-LMNCO	3.9	2.3	4.9364(5)	8.5550(4)	5.0251(1)	109.249(2)	200.35(2)

6. Refinement of structures with stacking faults with FAULTS[5]

Starting models for the structural refinements were adopted from Serrano-Sevillano *et al.*, where the conventional monoclinic Li_2MnO_3 unit cell was transformed into the triclinic system with $P\bar{1}$ space group.[6] Like in our previous publication[7], for $Li_{1.2}Mn_{0.6}Ni_{0.2}O_2$ and $Li_{1.2}Mn_{0.54}Ni_{0.13}Co_{0.13}O_2$, the TMs were approximated to Mn (i.e., $Li_{1.2}Mn_{0.6}Ni_{0.2}O_2$, $Li_{1.2}Mn_{0.54}Ni_{0.13}Co_{0.13}O_2$ → $Li_{1.2}Mn_{0.8}O_2$) to avoid overparameterization. B_{iso} is the isotropic thermal displacement parameter.

Table S9: Starting model for the structural refinement of Li_2MnO_3

Unit cell parameters						
	a, b (Å)		**c (Å)**		**γ (°)**	
	4.9265		4.7416		60.036	
Layer compositions						
Layer	**Atom**	**x/a**	**y/b**	**z/c**	**Occupancy**	**B_{iso}**
L1	Li	0	0	0	1	1
	Li	1/3	1/3	0	1	1
	Li	2/3	2/3	0	1	1
L2, L3 and L4	Li	0	0	0	1	1
	Mn	0	0	0	0	1
	Mn	1/3	1/3	0	1	1
	Li	1/3	1/3	0	0	1
	Mn	2/3	2/3	0	1	1
	Li	2/3	2/3	0	0	1
	O	0.340	0.000	0.225	1	1
	O	0.650	0.000	-0.225	1	1
	O	0.000	0.340	-0.225	1	1
	O	0.340	0.650	-0.225	1	1
	O	0.650	0.340	0.225	1	1
	O	0.000	0.650	0.225	1	1

Table S10: Starting model for the structural refinement of $Li_{1.2}Mn_{0.6}Ni_{0.2}O_2$ and $Li_{1.2}Mn_{0.54}Ni_{0.13}Co_{0.13}O_2$

Unit cell parameters						
	a, b (Å)		**c (Å)**		**γ (°)**	
	4.9265		4.7416		60.036	
Layer compositions						
Layer	**Atom**	**x/a**	**y/b**	**z/c**	**Occupancy**	**B_{iso}**
L1	Li	0	0	0	1	1
	Li	1/3	1/3	0	1	1
	Li	2/3	2/3	0	1	1
L2, L3 and L4	Li	0	0	0	0.6	1
	Mn	0	0	0	0.4	1
	Mn	1/3	1/3	0	0.9	1
	Li	1/3	1/3	0	0.1	1
	Mn	2/3	2/3	0	0.9	1
	Li	2/3	2/3	0	0.1	1
	O	0.340	0.000	0.225	1	1
	O	0.650	0.000	-0.225	1	1
	O	0.000	0.340	-0.225	1	1
	O	0.340	0.650	-0.225	1	1
	O	0.650	0.340	0.225	1	1
	O	0.000	0.650	0.225	1	1

To generate stacking faults, three different stacking vectors were used, (⅓, –⅓, 1/2), (⅔, 0, ½), and (0, –⅔, 1/2), each representing a distinct stacking of the Li-Mn-O layer with respect to the Li layer. Stacking faults were generated by varying the probability of occurrence of each of the vectors. The degree of faulting within the structure was calculated from the probability of the stacking vectors using the equation below:[8]

$$\text{Stacking fault probability (\%)} = \frac{1 - P_{L2}}{2/3} \times 100$$

where, P_{L2} is the probability of the occurrence of the L1→L2 transition.

Note that the translation probability of L1→L3 and L1→L4 transitions are always assumed the same.

6.1 FAULTS refinement results of the 900C-3h samples

The refinement methodology used is identical to that described in Serrano-Sevillano *et al*.[5] The background was manually selected. The scale factor, unit cell parameters, peak shape parameters, degree of faulting, and atomic positions (of Mn and O) were refined. The isotropic atomic displacement parameter (B_{iso}) was fixed to one for all atoms and not refined. The symmetric broadening of the Bragg reflections was modelled using the pseudo-Voigt peak shape function provided in the software. Definitions of the various refinement functions/parameters and the refinement metrics can be found in the FAULTS manual. Note that the software does not permit the modelling of the peak asymmetry due to axial divergence of the X-ray beam. As a result, accurate modelling of the most intense reflection, i.e., the 001 reflection at ~18.7° was not possible. This has partly contributed to the large refinement residual values. The refined values with the standard deviations in parentheses are tabulated below.

SG-LMO

Table S11: Refined structural parameters of SG-LMO.

R-Factor = 13.68 & χ^2 = 46.079						
Unit cell parameters & degree of faulting						
a, b (Å)		**c (Å)**		**γ (°)**		**Degree of faulting**
4.92145(1)		4.74004(2)		60.04601(19)		42.67(6)%
Atomic positions and occupancies						
Layer	**Atom**	**x/a**	**y/b**	**z/c**	**Occupancy**	**B_{iso}**
1	Li	0	0	0	1	1
	Li	1/3	1/3	0	1	1
	Li	2/3	2/3	0	1	1
2, 3 and 4	Li	0	0	0	1	1
	Mn	0.34003(16)	0.34003(16)	0	1	1
	Mn	0.67666(77)	0.67666(77)	0	1	1
	O	0.36819(62)	0.02179(27)	0.20815(45)	1	1
	O	0.64668(26)	0.00733(23)	−0.21333 (7)	1	1
	O	0.02211(2)	0.36813(1)	−0.20816(1)	1	1
	O	0.35738(21)	0.59535(9)	−0.17965(15)	1	1
	O	0.59510(1)	0.35725(1)	0.17953(1)	1	1
	O	0.00736(3)	0.64664(1)	0.21324(1)	1	1

SS-LMO (Multi-phase fit)

A satisfactory fit of the SS-LMO data was only obtained using multi-phase structural refinement using a faulted and fault-free phase Li_2MnO_3 phases, with the latter included as a background phase.

Table S12: Refined structural parameters of SS-LMO from a multi-phase fit.

R-Factor = 10.39 & χ^2 = 16.94						
Percentage area of phase - Faulted = 90.364% & Fault-free = 9.636%						
Unit cell parameters & degree of faulting						
a, b (Å)		**c (Å)**		**γ (°)**		**Degree of faulting in the faulted phase**
4.91977(2)		4.73754(2)		59.99860(12)		42.20(8)%
Atomic positions and occupancies						
Layer	**Atom**	**x/a**	**y/b**	**z/c**	**Occupancy**	**B_{iso}**
1	Li	0	0	0	1	1
	Li	1/3	1/3	0	1	1
	Li	2/3	2/3	0	1	1
2, 3 and 4	Li	0	0	0	1	1
	Mn	0.33311(17)	0.33311(17)	0	1	1
	Mn	0.66685(5)	0.66685(5)	0	1	1
	O	0.34137(79)	−0.00415(60)	0.23058(52)	1	1
	O	0.64775(8)	-0.00226(16)	-0.23144(2)	1	1
	O	-0.00417(3)	0.34136(1)	-0.23060(1)	1	1
	O	0.34996(22)	0.65143(10)	-0.22503(23)	1	1
	O	0.65126(2)	0.34975(2)	0.22501(1)	1	1
	O	-0.00224(4)	0.64777(1)	0.23142(1)	1	1

SS-LMO (Single-phase fit)

Table S13: Refined structural parameters of SS-LMO from a single-phase fit

R-Factor = 11.33 & χ^2 = 19.12						
Unit cell parameters & degree of faulting						
a, b (Å)		**c (Å)**		**γ (°)**		**Degree of faulting**
4.91966(1)		4.73770(2)		60.01423(10)		34.62(5)%
Atomic positions and occupancies						
Layer	**Atom**	**x/a**	**y/b**	**z/c**	**Occupancy**	**B_{iso}**
1	Li	0	0	0	1	1
	Li	1/3	1/3	0	1	1
	Li	2/3	2/3	0	1	1
2, 3 and 4	Li	0	0	0	1	1
	Mn	0.33292(9)	0.33292(9)	0	1	1
	Mn	0.66715(5)	0.66715(5)	0	1	1
	O	0.34471(65)	−0.00790(61)	0.23050(48)	1	1
	O	0.64396(5)	−0.00126(20)	−0.23242(3)	1	1
	O	−0.00803(2)	0.34480(1)	−0.23059(1)	1	1
	O	0.34451(21)	0.65159(8)	−0.22148(18)	1	1
	O	0.65126(2)	0.34450(2)	0.22142(1)	1	1
	O	−0.00116(4)	0.64399(1)	0.23236(1)	1	1

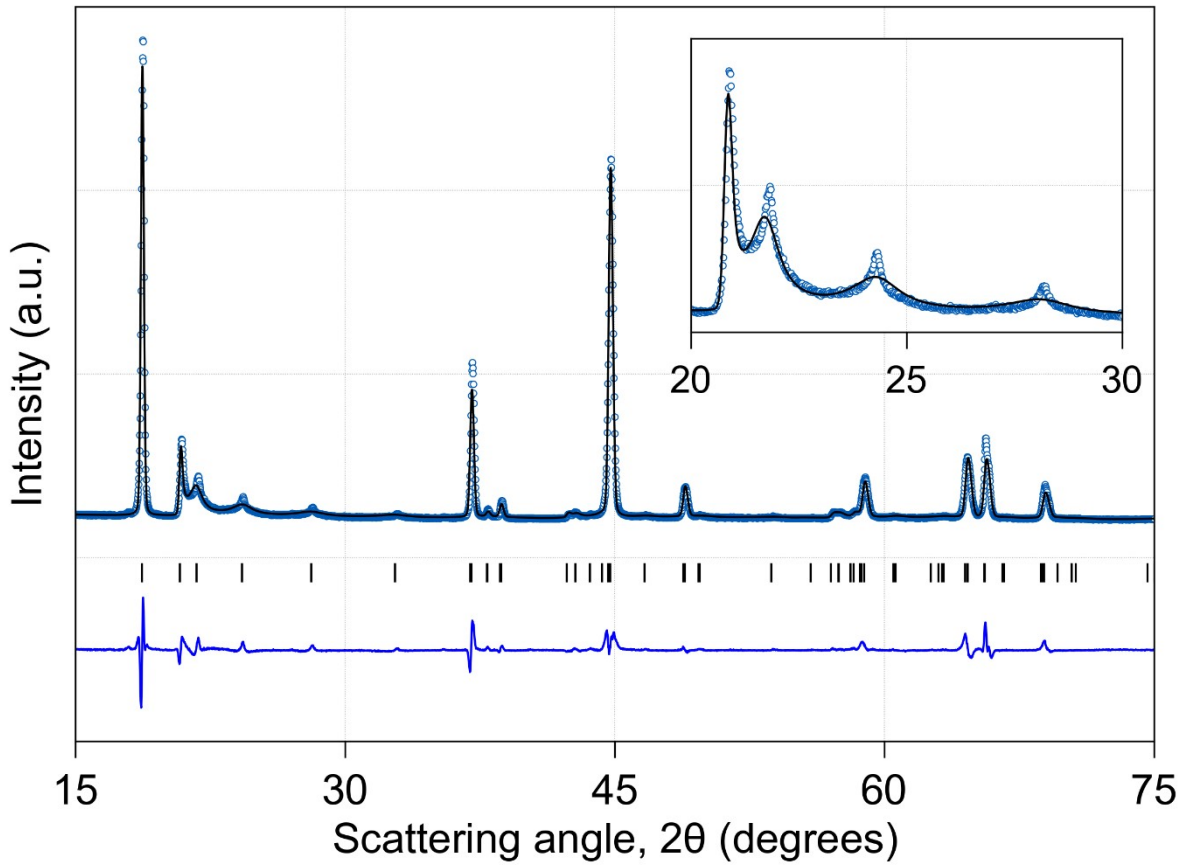

Figure S3: FAULTS refinement plot of SS-LMO with a single faulted phase

SG-LMNO

Table S14: Refined structural parameters of SG-LMNO.

R-Factor = 7.97 & χ^2 = 31.341						
Unit cell parameters & degree of faulting						
a, b (Å)		**c (Å)**		**γ (°)**		**Degree of faulting**
4.94983(2)		4.74999(2)		60.13999(19)		59.8(1)%
Atomic positions and occupancies						
Layer	**Atom**	**x/a**	**y/b**	**z/c**	**Occupancy**	**B_{iso}**
1	Li	0	0	0	1	1
	Li	1/3	1/3	0	1	1
	Li	2/3	2/3	0	1	1
2, 3 and 4	Li	0	0	0	0.6	1
	Mn	0	0	0	0.4	1
	Mn	0.37031(14)	0.37031(14)	0	0.9	1
	Li	0.37031(14)	0.37031(14)	0	0.1	1
	Mn	0.69191(23)	0.69191(23)	0	0.9	1
	Li	0.69191(23)	0.69191(23)	0	0.1	1
	O	0.39091(60)	0.01284(63)	0.23896(35)	1	1
	O	0.66974(67)	0.00821(56)	−0.21126(5)	1	1
	O	0.01297(4)	0.39192(2)	−0.23906(1)	1	1
	O	0.37646(23)	0.60166(12)	−0.17082(9)	1	1
	O	0.60119(1)	0.37617(2)	0.17041(1)	1	1

	O	0.00924(7)	0.66846(2)	0.21156(1)	1	1

CP-LMNO

Table S15: Refined structural parameters of CP-LMNO.

R-Factor = 5.37 & χ^2 = 12.15						
Unit cell parameters & degree of faulting						
a, b (Å)		**c (Å)**		**γ (°)**		**Degree of faulting**
4.95544(1)		4.7546(2)		59.9531(2)		36.76(7)%
Atomic positions and occupancies						
Layer	**Atom**	**x/a**	**y/b**	**z/c**	**Occupancy**	**B_{iso}**
1	Li	0	0	0	1	1
	Li	1/3	1/3	0	1	1
	Li	2/3	2/3	0	1	1
2, 3 and 4	Li	0	0	0	0.6	1
	Mn	0	0	0	0.4	1
	Mn	0.34266(18)	0.34266(18)	0	0.9	1
	Li	0.34266(18)	0.34266(18)	0	0.1	1
	Mn	0.67640(16)	0.67640(16)	0	0.9	1
	Li	0.67640(16)	0.67640(16)	0	0.1	1
	O	0.36577(72)	−0.02180(43)	0.23691(39)	1	1
	O	0. 65586(23)	−0.02967(18)	−0.24136(4)	1	1
	O	−0.01902(6)	0.36674(3)	−0.23669(1)	1	1
	O	0. 35837(28)	0.63833(35)	−0.23620(8)	1	1
	O	0.63716(3)	0.35593(3)	0.23650(1)	1	1
	O	−0.03109(2)	0.65427(2)	0. 24301(1)	1	1

SG-LMNCO

Table S16: Refined structural parameters of SG-LMNCO.

R-Factor = 6.11 & χ^2 = 19.352						
Unit cell parameters & degree of faulting						
a, b (Å)		**c (Å)**		**γ (°)**		**Degree of faulting**
4.93329(2)		4.72935(3)		59.98946(13)		58.3(1)%
Atomic positions and occupancies						
Layer	**Atom**	**x/a**	**y/b**	**z/c**	**Occupancy**	**B_{iso}**
1	Li	0	0	0	1	1
	Li	1/3	1/3	0	1	1
	Li	2/3	2/3	0	1	1
2, 3 and 4	Li	0	0	0	0.6	1
	Mn	0	0	0	0.4	1
	Mn	0.37013(12)	0.37013(12)	0	0.9	1
	Li	0.37013(12)	0.37013(12)	0	0.1	1
	Mn	0.68699(28)	0.68699(28)	0	0.9	1
	Li	0.68699(28)	0.68699(28)	0	0.1	1
	O	0.36373(86)	0.02057(82)	0.24619(39)	1	1
	O	0.67152(75)	−0.01782(33)	−0.20783(21)	1	1
	O	0.02060(4)	0.36360(1)	−0.24639(1)	1	1
	O	0.3678(4)	0.61582(14)	−0.16718(9)	1	1
	O	0.61596(1)	0.36793(2)	0.16717(1)	1	1
	O	−0.01707(757)	0.67149(2)	0.20776(1)	1	1

CP-LMNCO

Table S17: Refined structural parameters of CP-LMNCO.

R-Factor = 4.11 & χ^2 = 12.382						
Unit cell parameters & degree of faulting						
a, b (Å)		**c (Å)**		**γ (°)**		**Degree of faulting**
4.93793(1)		4.74865(2)		59.97823(18)		43.8(3)%
Atomic positions and occupancies						
Layer	**Atom**	**x/a**	**y/b**	**z/c**	**Occupancy**	**B_{iso}**
1	Li	0	0	0	1	1
	Li	1/3	1/3	0	1	1
	Li	2/3	2/3	0	1	1
2, 3 and 4	Li	0	0	0	0.6	1
	Mn	0	0	0	0.4	1
	Mn	0.33381(20)	0.33381(20)	0	0.9	1
	Li	0.33381(20)	0.33381(20)	0	0.1	1
	Mn	0.66665(22)	0.66665(22)	0	0.9	1
	Li	0.66665(22)	0.66665(22)	0	0.1	1
	O	0.34389(73)	−0.02513(33)	0.23890(37)	1	1
	O	0.62876(8)	−0.01372(12)	−0.24873(4)	1	1
	O	−0.02506(2)	0.34391(2)	−0.23889(1)	1	1
	O	0.32337(27)	0.66058(30)	−0.22286(6)	1	1
	O	0.66058(2)	0.32334(2)	0.22285(1)	1	1
	O	−0.01378(2)	0.62870(1)	0.24880(1)	1	1

References

1. Whitfield, P.; Davidson, I.; Stephens, P.; Cranswick, L.; Swainson, I., Diffraction analysis of the lithium battery. *Zeitschrift fuer Kristallographie Suppl.* **2007,** *26*, 483–488.
2. Coelho, A. A., TOPAS and TOPAS-Academic: An optimization program integrating computer algebra and crystallographic objects written in C++. *Journal of Applied Crystallography* **2018,** *51* (1), 210–218.
3. Balzar, D.; Audebrand, N.; Daymond, M. R.; Fitch, A.; Hewat, A.; Langford, J. I.; Le Bail, A.; Louer, D.; Masson, O.; McCowan, C. N.; Popa, N. C.; Stephens, P. W.; Toby, B. H., Size-strain line-broadening analysis of the ceria round-robin sample. *Journal of Applied Crystallography* **2004,** *37* (6), 911–924.
4. Pawley, G., Unit-cell refinement from powder diffraction scans. *Journal of Applied Crystallography* **1981,** *14* (6), 357–361.
5. Casas-Cabanas, M.; Reynaud, M.; Rikarte, J.; Horbach, P.; Rodriguez-Carvajal, J., FAULTS: A program for refinement of structures with extended defects. *Journal of Applied Crystallography* **2016,** *49*(6), 2259–2269.
6. Serrano-Sevillano, J.; Reynaud, M.; Saracibar, A.; Altantzis, T.; Bals, S.; van Tendeloo, G.; Casas-Cabanas, M., Enhanced electrochemical performance of Li-rich cathode materials through microstructural control. *Physical Chemistry Chemical Physics* **2018,** *20*(35), 23112–23122.
7. Menon, A. S.; Ulusoy, S.; Ojwang, D. O.; Riekehr, L.; Didier, C.; Peterson, V. K.; Salazar-Alvarez, G.; Svedlindh, P.; Edström, K.; Gomez, C. P.; Brant, W. R., Synthetic Pathway Determines the Nonequilibrium Crystallography of Li- and Mn-Rich Layered Oxide Cathode Materials. ACS Applied Energy Materials **2021**, *4*(2), 1924–1935.
8. Shunmugasundaram, R.; Arumugam, R. S.; & Dahn, J. R., A study of stacking faults and superlattice ordering in some Li-rich layered transition metal oxide positive electrode materials. *Journal of The Electrochemical Society* **2016**, *163*(7), A1394.